Geosci. Instrum. Method. Data Syst. Discuss., 2, 643–656, 2012
www.geosci-instrum-method-data-syst-discuss.net/2/643/2012/
doi:10.5194/gid-2-643-2012

Discussions Geoscientific Instrumentation Methods and Data Systems

Evaluation of positioning and density profiling accuracy of muon radiography by utilizing a 15-ton steel block

H. K. M. Tanaka

Earthquake Research Institute, the University of Tokyo, Tokyo, Japan

Received: 29 June 2012 – Accepted: 1 August 2012 – Published: 21 August 2012

Correspondence to: H. K. M. Tanaka (ht@riken.jp)

Published by Copernicus Publications on behalf of the European Geosciences Union.

Abstract

A model experiment was performed in order to evaluate the spatial resolution and accuracy of determining density by utilizing steel blocks whose density ($7.8\,g\,cm^{-3}$) and geometrical structure (5 m in length and 40 cm in width) were both well known. By comparing the experimental result with simulations, a density and a width of the steel block were measured as $7.3 \pm 1.0\,g\,cm^{-3}$ and 37 ± 15 cm, respectively.

1 Introduction

Muon radiography was first proposed to determine a thickness of an overburden of a horizontal tunnel in the Snowy Mountains in Australia (George, 1955). He measured the muon flux inside and outside the tunnel to compare them to confirm that a reduction in the muon flux reflects the average density of the overburden. In his experiment, he compared the muon data with the core sampling data, and concluded that they were consistent each other within error bars of ~ 10 %. The method measures the absorption of muons along a cross section of the target volume volcano parallel to the plane of the detector, on which the average density along all muon paths is projected. The amount of energy lost by muons while passing through matter is dependent on the density of that matter. The resultant angular distribution of the muons can then be used to calculate the density profile of the target volume a volcano. The change in the muon angle after they passes through a substantial mass gigantic matter is very small (12 mrad for SiO_2 with a thickness of 1.5 km). Muon radiography consequently constitutes a unique way to obtain direct information on the density distribution of geological objects with accuracy in terms of spatial resolution that is superior to that possible using conventional geophysical techniques.

The muon is the most numerous of the charged elementary particles at sea level and is capable of traveling large distances through matter. They arrive at angles ranging from the vertical to the horizontal with an integral intensity of $70\,m^{-2}\,s^{-1}\,sr^{-1}$ at sea

GID

2, 643–656, 2012

level. Thus, cosmic-ray muon radiography can be applied to any objects located elevations vertically above where the detector is placed. Since George's first muon radiography, researchers have been attempting to image pyramids (Alvarez et al., 1970), ore bodies (Malmqvist et al., 1979), volcanoes (Tanaka et al., 2007, 2008; Lesparre et al., 2012), seismic faults (Tanaka et al., 2011), caves (Caffau et al., 1996), and archaeological sites (Basset et al., 2006; Menichelli et al., 2007) radiographically using cosmic-ray muons. However, accuracy in positioning and determining density has not been quantitatively estimated. In this work, these important parameters have been evaluated by using a large steel block whose density and geometry are both well known.

2 Muon detector

Conventionally, a combination of plastic scinitillator strips has been used to assemble two segmented scintillation detector planes to track muon trails (Tanaka et al., 2009; Ambrosi et al., 2011) because a plastic-scintillator requires a minimal maintenance, has low power consumption, and is relatively insensitive to ambient conditions. Each scintillator strip is coupled with a photomultiplier tube (PMT). A PMT provides high photon sensitivity and fast response to scintillation light, and thus, the signal of the PMT can be used as the trigger for timing. In a multianode PMT (MAPMT), PMTs are combined so that signals can be treated collectively, and the scintillator strip does not have to be separated into units. Although it is difficult to continue observations when one MAPMT breaks because the detector consists of an integrated combination of scintillators and MAPMTs, its construction can be more robust and better suited for a certain outdoor environment.

In this work, a segmented muon detection system (Tanaka et al., 2009) was utilized. The system consists of plastic scintillator strips, PMTs, and readout electronics. The size of scintillator strip (Bicron BC-408) is 30 cm (L) × 2.5 cm (W) × 1.5 cm (H). The plane contains 24 plastic scintillators arranged along the x and y coordinates like a lattice, to determine the vertex point by determining the coincidence of two signals from

GID
2, 643–656, 2012

two scintillator strips; it consists of 144 coincident elements. The total area of the plane is 0.09 m^2, and the unit weighs ~ 10 kg. A slot (2 mm in depth and 2 mm in width) in the plastic scintillator contains a wavelength-shifting (WLS) fiber with a diameter of 1 mm (Bicron BCF-91A). The fiber converts purple scintillation light (wavelength ~ 420 nm) into green light (wavelength ~ 500 nm), and conveys the optical signal to an MAPMT. This WLS can transmit light without greatly attenuating it because there is a clad layer outside of the fiber as well as an optical fiber. The end of the fiber is held by a black colored holder; black silicon rubber is affixed between the fiber and the fiber holder to prevent light leakage. The fiber holder and the MAPMT (HAMAMATSU H8500) are fastened together with light shielding tape. The H8500 MAPMT has 64 anode pixels. While the quantum efficiency of the PMT is 24 % for standard scintillation light, the quantum efficiency is 14 % for the light emitted from the WLS fiber. The quantum efficiency of light emitted from a WLS fiber is therefore 57 % compared with that of the usual scintillation light.

When MAPMT was supplied 870 V of electric power, the typical peak of the pulse height output from MAPMT was 80 mV, and the pulse width was 2 ns. We measured total electric power consumption of the muon detection system with the MAPAMT by using a power meter (HIOKI 3334 AC/DC POWER HITESTER), and confirmed it was 9 W including the power consumption by electronics.

3 Model experiment

The purpose of the experiment was to estimate accuracy in positioning and determining density by using a steel block whose density and geometry are both well known. The procedure includes (1) an estimate of accuracy in determining density by assuming the geometry of the steel block is known, and (2) an estimate of accuracy in positioning by assuming the density of the steel block is known. With this goal, we measured the muon flux using the MAPMT detector and compared the experimental result with a Geant4 simulation assuming the DEIS flux (Allkofer et al., 1981). The experimental

GID
2, 643–656, 2012

setup is shown in Fig. 1a. The size of the steel block is 5 m in length and 40 cm in width and weighs ∼ 15 tons. Its density is 7.8 g cm^{-3}. The steel block was supported by the metal plate with a thickness of 30 mm for the purpose of force dispersion. This metal plate was further supported by a concrete block with a thickness of 300 mm in order to prevent land subsiding. The distance between the center of gravities of the steel block and the detection system is ∼ 5 m. The distance between two segmented scintillation detector planes was 75 cm, and a root means square (RMS) angular resolution of the system was ± 14 mrad at an angular interval of 33 mrad. An RMS angular resolution ($\Delta\theta_{\mathrm{res}}$) is a minimum resolvable angle of the detector, and the angular interval ($\Delta\theta_{\mathrm{int}}$) is a value that is defined by the width of the scintillator strips (d) and the distance between two detector planes (L); d/L. $\Delta\theta_{\mathrm{res}}$ and $\Delta\theta_{\mathrm{int}}$ have the following relationship $(\Delta\theta_{\mathrm{int}} - \Delta\theta_{\mathrm{res}})^2/\Delta\theta_{\mathrm{int}}^2 = 0.32$. The muon data were compiled and analyzed by a network-based FPGA (field programmable gate array) muon read out electronics (Uchida et al., 2010). The FPGA works on a 50-MHz system clock. The event filter (which selects events that can be used to construct the muon paths and generates path information), the histogram generator, and the network processor are implemented on the single FPGA. The PMT signals analyzed in the FPGA chip are recorded in a number of bins representing the azimuth and elevation arriving angles of cosmic ray muons. The data were read by the network processor when a remote PC accesses the electronics. The observation period was one month.

In order to compare the experimental result with simulations, we performed Monte Carlo simulations by taking the following steps.

1. 3-D geometrical information of the steel block was used to obtain the path length in the direction of θ and ϕ, as seen from the muon detector by constructing a virtual detection system in a computer.

2. We generated random numbers, and using these numbers, we generated muons adapted to the energy distribution obtained by Eq. (1).

GID
2, 643–656, 2012

3. The generated muons were injected into a steel block with a thickness of X (m) in order to calculate the stopping length of the muons in the target by using Geant4 (Agostinelli et al., 2003), and a table $N(\theta, X)$ was constructed to represent the data.

4. By using the result of (1) and (3), we calculated the number of muons during a 30-day measurement period counted in direction of θ and ϕ.

4 Results and discussions

The result of a 30-day measurement period is shown in Fig. 2. The number of muon events counted within the different elevation angular regions of 95 mrad $< \theta <$ 158 mrad and 190 mrad $< \theta <$ 285 mrad are plotted with bars solid squares and crosses circles respectively. The whole area of the detection system is sensitive to muons that arrive come from near horizontally, but the system does not catch all the muons that enter at large angles to the horizontal. As shown in Fig. 2, the system has a geometrical acceptance, which the horizontal distributions of muons can be used to correct. In this figure, the geometrical acceptance was corrected for the elevation angles. The muons with angles 190–285 mrad have not passed through the block, while those with angles 95–158 have. The plots for 190 mrad $< \theta <$ 285 mrad show the data without a target object, and the results confirmed the integral muon intensity as can be calculated by Eq. (1). For 95 mrad $< \theta <$ 158 mrad, significant decreases in events can be seen between $\phi = 0$ and 66 mrad, primarily due to increases in the average density along the muon paths coming from an existence of the steel block.

This result was compared with the Geant4 Monte Carlo simulations (solid lines in Fig. 2), which give the integrated flux of muons at various azimuth angles penetrating through a given density length (density × path length) by referring to the geometry of the steel block. The simulations were performed by assuming the uniform average density values that ranges from 0 to 13 g cm^{-3}. From the comparison between the

GID
2, 643–656, 2012

experimental and simulation result, the average density of the steel block was determined as $7.3 \pm 1.0\,\mathrm{g\,cm^{-3}}$ at a 1σ confidence level. Figure 3 shows the integrated flux of muons penetrating through a given geometry of the steel block by referring to the average density of the steel block, which was determined in the previous procedure. By comparing the data with the simulation results for different widths of the steel block, which ranges from 10 to 60 cm, the width was determined as 37 ± 15 cm at a 1σ confidence level.

In this experiment, the density of the steel block was determined as $7.3 \pm 1.0\,\mathrm{g\,cm^{-3}}$, therefore, the accuracy in determining density is 13 %. The typical energy of muons at sea level is 3–4 GeV, sufficient to penetrate meters of steel block. Most of the muons transmit the steel block and thus, the absorption rate is not very sensitive insensitive to the target density. However, if we perform a similar experiment using a km rock, the absorption rate can be more sensitive to the target density, and as a result, the accuracy can be improved. Figure 4 shows a simulation result of the sensitivity of the muon transmission rate to the target density for different path lengths. The simulation compares the transmission rate between a km rock ($\rho = 2\,\mathrm{g\,cm^{-3}}$) and a 5-m steel block ($\rho = 7.9\,\mathrm{g\,cm^{-3}}$). Since the low energy muon flux is screened by the target volume, a density can be more precisely determined for a thicker larger target. The statistical error in the measured number of muons in the present experiment was ± 2 %. For this variation, we can calculate that the accuracy in determining the density of a km of rock is ± 1 %, whereas that for a 5-m steel block is ± 13 %. The statistic error we measured in the present experiment was ± 2 %. For this error bar, we can calculate that the accuracy in determining density is ± 1 % for a km rock whereas that for a 5-m steel block is ± 13 %.

An RMS angular resolution of the present system is ($\Delta\theta_{\mathrm{res}}$, $\Delta\phi_{\mathrm{res}} = \pm 14$ mrad, ± 14 mrad) at an angular interval of 33 mrad. The minimum resolvable distance (MRD) (spatial resolution ΔX_{res}, ΔY_{res}) at the target volume (in this case, an Fe block) is defined by the minimum resolvable angle of the detector (in this case, an RMS angular resolution) ($\Delta\theta_{\mathrm{res}}\,\Delta\phi_{\mathrm{res}}$) and the distance between the target and the detector (R);

GID
2, 643–656, 2012

$(\Delta X_{res}, \Delta Y_{res}) = R \times (\Delta\theta_{res}, \Delta\phi_{res})$. The spatial interval $(\Delta X_{int}, \Delta Y_{int})$ at the target volume is defined by the angular interval of the detector $(\Delta\theta_{int}\,\Delta\phi_{int})$ and the distance between the target and the detector (R); $(\Delta X_{int}, \Delta Y_{int}) = R \times (\Delta\theta_{int}, \Delta\phi_{int})$. Therefore we expect that the theoretical MRD will be ± 7.0 cm with a spatial interval of 16.5 cm in the present case. In this work, the actual minimum resolvable distance ($\Delta X = 15$ cm) was measured between the theoretical MRD and the spatial interval:

$$\Delta X_{res} < \Delta X < \Delta X_{int}. \quad (1)$$

Equation (1) confirms that the theoretical MRD (RMS angular resolution) of the segmented muon detection system approximately equals to the actual MRD (or spatial resolution) at the target. Tanaka et al. (2007, 2008, 2009, 2011) and Lesparre et al. (2012) used one half of the spatial interval as the minimum resolvable distance. They both used a segmented muon detection system. Their approaches were validated by this work.

5 Conclusions

Accuracy of positioning and determining densities in muon radiography was first quantitatively evaluated by utilizing a steel block. In the present experiment, we measured an accuracy of 13 % in determining a density of a steel block with a length of 5 m, and based on this value, we confirmed that the accuracy will be improved to 1 % when the target is a rock with a thickness of 1 km. Also, we confirmed that the positioning resolution depends on the segmentation geometry of the muon detector, and it was determined between a RMS angular resolution and an interval angle of the detection system.

Acknowledgements. The experiment was supported by a collaborative research between Nippon Steel Corporation and University of Tokyo. Analysis and simulation works greatly benefited from the skill expertise of Hideaki Taira. This work greatly benefited from suggestions by Tony Hurst and anonymous reviewers.

GID
2, 643–656, 2012

References

Allkofer, O. C., Carstensen, K., Dau, W. D., Jokisch, H., Klemke, G., Oren, Y., Uhr, R. C., and Bella, G.: Muon Spectra from DEIS up to 7 TeV, Proc. of 17th Cosmic Ray Conf., Paris, 10, 321, 1981.

Alvarez, L. W., Anderson, J. A., Bedwei, F. E., Burkhard, J., Fakhry, A., Girgis, A., Goneid, A., Hassan, F., Iverson, D., Lynch, G., Miligy, Z., Mousaa, A. H., Sharkawi, M., and Yazolinio, L.: Search for hidden chambers in the pyramids, Science, 167, 832-839, 1970.

Ambrosi, G., Ambrosino, F., Battiston, R., Bross, A., Callier, S., Cassese, F., Castellini, G., Ciaranfi, R., Cozzolino, F., D'Alessandro, R., de La Taille, C., Iacobucci, G., Marotta, A., Masone, V., Martini, M., Nishiyama, R., Noli, P., Orazi, M., Parascandolo, L., Parascandolo, P., Passeggio, G., Peluso, R., Pla-Dalmau, A., Raux, L., Rocco, R., Rubinov, P., Saracino, G., Scarpato, G., Sekhniaidze, G., Strolin, P., Tanaka, H. K. M., Tanaka, M., Trattino, P., Uchida, T., and Yokoyamao, I.: The MU-RAY project: Volcano radiography with cosmic-ray muons, Nucl. Instrum. Meth. Phys. Res. Sect. A, 628, 120–123, 2011.

Basset, M., Ansoldi, S., Bari, M., Battiston, R., and Blasko, S.: MGR: An innovative, low-cost and compact cosmic-ray detector, Nucl. Instrum. Meth. Phys. Res. A, 567, 298–301, 2006.

Caffau, E., Coren, F., and Giannini, G.: Underground cosmic-ray measurement for morphological reconstruction of the "Grotta Gigante" natural cave, Nucl. Instrum. Meth. Phys. Res. A, 385, 480–488, 1997.

George, E. P.: Cosmic rays measure overburden of tunnel, Commonwealth Engineer, 1 July, 455–457, 1955.

Lesparre, N., Gibert, D., Marteau, J., Komorowski, J.-C., Nicollin, F., and Coutant, O.: Density muon radiography of La Soufrière of Guadeloupe volcano: comparison with geological, electrical resistivity and gravity data, Geophys. J. Int., 190, 1008–1019, doi:10.1111/j.1365-246X.2012.05546.x, 2012.

Malmqvist, L., J¨onsson, G., Kristiansson, K., and Jacobsson, L.: Theoretical studies of in-situ rock density determination using cosmic-ray muon intensity measurements with application in mining geophysics, Geophysics, 44, 1549–1569, 1979.

Menichelli, M., Ansoldi, S., Bari, M., Basset, M., and Battiston, R.: A scintillating fibres tracker detector for archaeological applications, Nucl. Instrum. Meth. Phys. Res. A, 572, 262–265, 2007.

GID
2, 643–656, 2012

Tanaka, H. K. M., Nakano, T., Takahashi, S., Yoshida, J., Takeo, M., Oikawa, J., Ohminato, T., Aoki, Y., Koyama, E., Tsuji, H., and Niwa, K.: High resolution imaging in the inhomogeneous crust with cosmic ray muon radiography: The density structure below the volcanic crater floor of Mt. Asama, Japan, Earth Planet. Sc. Lett., 263, 104–113, 2007.

Tanaka, H. K. M., Nakano, T., Takahashi, S., Yoshida, J., Takeo, M., Oikawa, J., Ohminato, T., Aoki, Y., Koyama, E., Tsuji, H., Ohshima, H., Maekawa, T., Watanabe, H., and Niwa, K.: Radiographic imaging below a volcanic crater floor with cosmic-ray muons, Am. J. Sci., 308, 843–850, 2008.

Tanaka, H. K. M., Uchida, T., Tanaka, M., Shinohara, H., and Taira, H.: Cosmic-ray muon imaging of magma in a conduit: Degassing process of Satsuma-Iwojima Volcano, Japan, Geophys. Res. Lett., 36, L01304, doi:10.1029/2008GL036451, 2009.

Tanaka, H. K. M., Miyajima, H., Kusagaya, T., Taketa, A., Uchida, T., and Tanaka, M.: Cosmic muon imaging of hidden seismic fault zones: Rainwater permeation into the mechanical fractured zones in Itoigawa-Shizuoka Tectonic Line, Japan, Earth Planet. Sc. Lett., 306, 156–162, 2011.

GID

2, 643–656, 2012

Positioning and density profiling accuracy of muon radiography

H. K. M. Tanaka

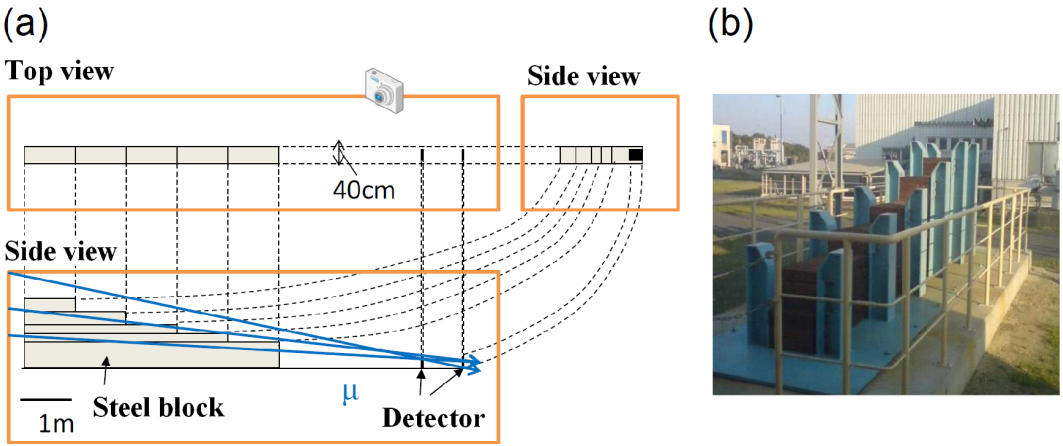

Fig. 1. Schematic view of the experimental setup **(a)** and a photograph of a 15-ton steel block **(b)**.

GID
2, 643–656, 2012

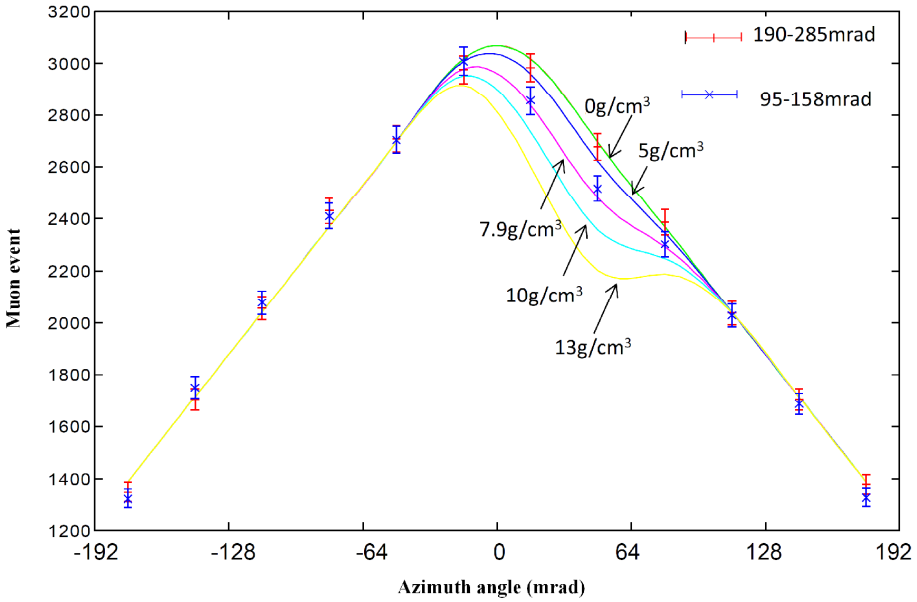

Fig. 2. Muon event as a function of azimuth angles counted within different elevation angle regions ($95 < \theta < 158$ mad and $190 < \theta < 285$ mrad). Monte-Carlo simulation results for different uniform densities (0, 5, 7.9, 10 and 13 g cm^{-3}) are overlaid on the data.

GID
2, 643–656, 2012

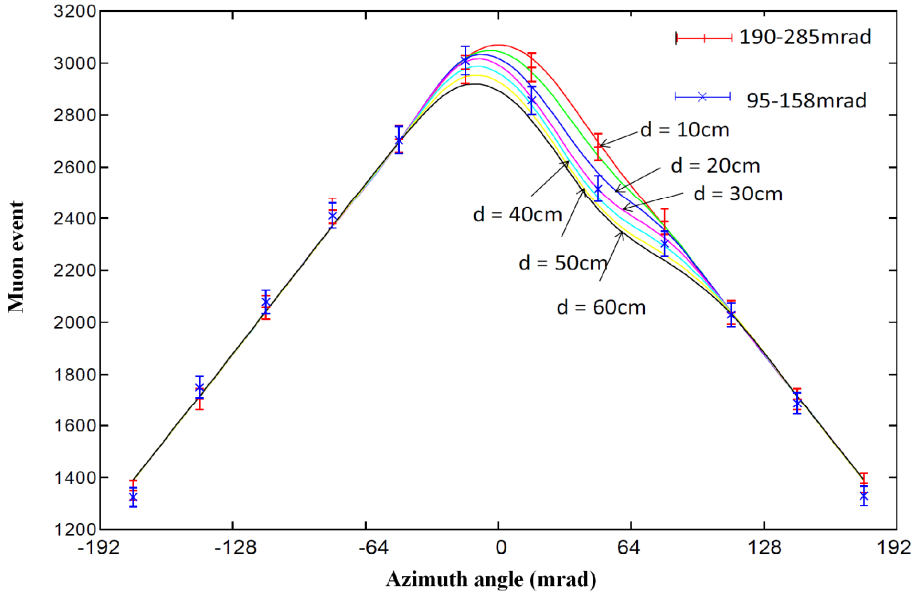

Fig. 3. Muon event as a function of azimuth angles counted within different elevation angle regions ($95 < \theta < 158$ mad and $190 < \theta < 285$ mrad). Monte-Carlo simulation results for various widths (10, 20, 30, 40, 50 and 60 cm) of the steel block are overlaid on the data.

GID
2, 643–656, 2012

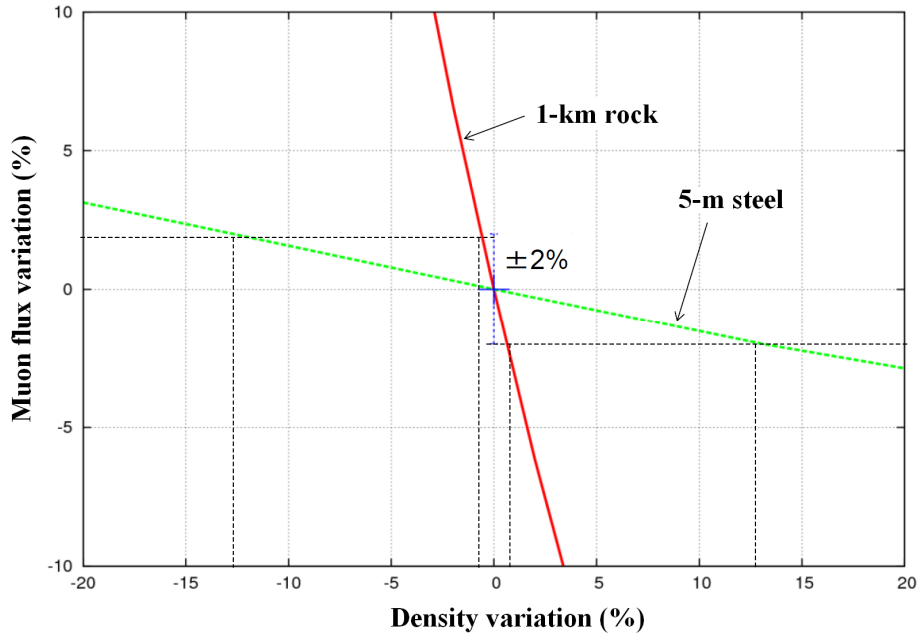

Fig. 4. Simulation results of the sensitivity of the muon transmission rate to the target density for different path lengths.

GID
2, 643–656, 2012